Korean J. Chem. Eng., **31**(9), 1564-1569 (2014)
DOI: 10.1007/s11814-014-0091-6

pISSN: 0256-1115
eISSN: 1975-7220

Comparison of CuO-MO_x (M=Ce, Zn, Cr and Zr) catalysts in various water-gas shift reactions

Enakonda Linga Reddy, Sang Yoon Kim, Mamilla Jhansi Lakshmi Kishore, Hyun Chan Lee, and Dong Hyun Kim†

Department of Chemical Engineering, Kyungpook National University, Daegu 702-701, Korea
(*Received 30 December 2013 • accepted 25 March 2014*)

Abstract−The water-gas shift (WGS) reaction in the temperature range of 100-350 °C for various feed compositions simulating forward, reverse and real WGS conditions was studied for a series of coprecipitated mixed metal oxide catalysts of 30 wt% of CuO and 70 wt% of metal oxide (CeO_2, ZnO, Cr_2O_3, and ZrO_2) as well as for a commercial WGS catalyst (ICI 83-3). The catalysts were characterized using BET, XRD, H_2-TPR and N_2O dissociation studies. Among the tested catalysts, CuO-Cr_2O_3 showed the best activity in the forward WGS, while the commercial catalyst was the best catalyst in the real and reverse WGS reactions. The effect of Cu content in the catalyst was also studied and, in the case of the real WGS, 50 wt% CuO-Cr_2O_3 was more active than 30 wt% CuO-Cr_2O_3. H_2 and CO_2 were found to inhibit the forward WGS, decreasing the reaction rate substantially, particularly at temperatures below 200 °C. The inhibition effect varied depending on the tested catalyst and increased with increasing H_2 or CO_2 concentration. As the inhibition effect was reversible, the competitive adsorption of H_2 or CO_2 on the active sites has been suggested to be responsible for the effect. The high activity of the commercial catalyst in the H_2 rich real WGS could be described by the difference in the H_2 inhibition between the catalysts. An easily reducible copper species was found in CuO-Cr_2O_3 and could be attributed to the high activity in the forward WGS.

Keywords: Mixed Metal Oxide Catalysts, Water Gas Shift Reaction, H_2 Inhibition, CO_2 Inhibition, Copper Chromate Catalyst

INTRODUCTION

The water-gas shift (WGS) reaction is not only important for generating hydrogen, but also useful for enriching hydrogen in the effluent stream of reforming units by decreasing the concentration of CO [1-5]. This is often a two-stage process: the high-temperature shift (HTS) over 350 °C and the low-temperature shift (LTS) below 250 °C. The standard industrial catalysts for these processes are iron oxide promoted with chromium oxide for the HTS step, and copper on a mixed support composed of zinc oxide and aluminum oxide for the LTS step [6,7]. The WGS reaction is reversible and mildly exothermic, and hence, is thermodynamically unfavorable at elevated temperatures. Therefore, the equilibrium conversion of CO is dependent largely on the reaction temperature, and a lower temperature is favored for higher CO removal [1,8-10].

$$CO+H_2O \leftrightarrow CO_2+H_2,\ \Delta H=-41.1\ kJ/mol,\ \Delta G=-28.6\ kJ/mol \quad (1)$$

CuO-CeO_2 has been reported to be an active catalyst for the WGS reaction [2,11-14]. Wang et al. [15] studied the behavior of CuO_x-CeO_2 and $Ce_{1-x}Cu_xO_2$ catalysts for the WGS reaction, identifying the active sites on Cu-CeO_2 catalyst and illustrating the importance of *in-situ* structural studies for the WGS reaction. It has been reported that, CuO-ZrO_2 catalyst showed a good performance in the forward WGS conditions, namely in the absence of the product components, ie, H_2 and CO_2 [16,17]. Shishido et al. [18] studied ZnO based Cu catalyst for the WGS reaction, reporting that the binary catalysts (Cu-ZnO) showed higher activity than the ternary catalysts (Cu-ZnO/Al_2O_3), and that this activity may depend on the copper metal surface area of the catalyst. Boumaza et al. [19] studied a series of CuM_2O_4 (where M is Al, Zn, Mn, Co, Cr and Fe) spinel catalysts for water gas shift reaction at atmospheric pressure and reported $CuCr_2O_4$ as the best catalyst among the series. Significant improvements in the activity of skeletal copper catalysts for the WGS reaction were achieved by adding small amounts of Cr_2O_3 to the copper surface [20]. The stability and the activity of Cr_2O_3 supported catalysts were examined by Park et al. [21] for a reverse WGS reaction, who reported that the Cr_2O_3 supported catalyst activity was stable during the reverse WGS reaction and no coke was formed during the reaction. The literature on WGS clearly shows that the activity of the Cu-based catalysts can be considerably improved when combined with the metal oxides, namely CeO_2, ZnO, ZrO_2 and Cr_2O_3.

Hence, we attempted to directly compare the performance of the mixed metal oxide catalysts (CuO-CeO_2, CuO-ZnO, CuO-Cr_2O_3 and CuO-ZrO_2) on WGS reactions. To characterize the catalysts, we made BET, XRD, H_2-TPR and N_2O dissociation measurements for the catalysts. To investigate the catalytic performance under various WGS conditions, we tested the catalysts for three different feed conditions: forward WGS (CO and H_2O), reverse WGS (CO_2 and H_2) and real WGS (CO, H_2O, CO_2 and H_2).

EXPERIMENTAL

1. Catalyst Preparation

Binary mixed metal oxide catalysts of 30 wt% CuO and 70 wt% metal oxide (CeO_2, ZnO, Cr_2O_3, or ZrO_2) were prepared by co-precipitation. The nitrate salts of copper and the partner metal (i.e., Ce,

†To whom correspondence should be addressed.
E-mail: dhkim@knu.ac.kr

Zn, Cr, or Zr) were dissolved in deionized water. Precipitation with a solution of 1.0 M NaOH was carried out at pH 10 and 50 °C under vigorous stirring for 1 h. The resulting precipitate was filtered and washed with hot deionized water to remove sodium ions until the pH of the filtrate was 7. The precipitate was dried for 10 h at 80 °C and calcined in a muffle furnace for 3 h at 500 °C. The calcined catalysts were ground and sieved to 250-425 μm in size.

2. Catalytic Activity Measurements

The water-gas shift reaction was carried out in a fixed bed reactor over a temperature range of 100-350 °C at atmospheric pressure. The reactor was a ¼-inch quartz tube, into which 1 g of catalyst with the size of 250-425 μm was loaded. Prior to the activity test, the catalyst was reduced for 2 h at 300 °C in a 10% H_2/He gas flowing at 50 mL/min. The catalyst bed was then cooled to 100 °C in a He atmosphere before the reaction was started. In the reaction experiments, the reactor temperature was slowly increased from 100 °C to 350 °C at a rate of 0.5 °C/min and, after reaching 350 °C, it was cooled under He flow to 100 °C before the next run of the same catalyst. All the feed gases were of UHP grade and were further purified with oxygen and a water trap (except CO). The iron carbonyl impurity from CO was decomposed by passing the CO stream through a trap at 400 °C.

Experiments were carried out at three feed compositions:

(i) forward WGS (5% CO, 15% H_2O and balance He)

(ii) real WGS (5% CO, 15% H_2O. 40% H_2, 10% CO_2 and balance He)

(iii) reverse WGS (40% H_2, 10% CO_2 and balance He)

The total feed flow rate was 50 mL/min and the reaction products were analyzed by gas chromatography (GC, Agilent 6890N) equipped with a TCD detector.

3. Catalyst Characterization

Specific surface areas of the fresh catalysts were measured by BET method (Micromeritics ASAP 2010). XRD patterns of the fresh and used catalysts were determined with a Rigaku powder diffractometer (D/Max-2500), utilizing Cu-Kα radiation in the 2θ range of 20-80. The reduction profiles of the prepared catalysts were measured by the H_2-TPR method at atmospheric pressure in a conventional flow system with a temperature ramp of 10 °C/min from 50 to 400 °C. A 50 mg sample was placed in a U-shaped quartz tube which was heated in a furnace under a flow of 10% H_2 in N_2 stream at 50 mL/min. Before each measurement, the samples were purged in a flow of N_2 at 250 °C for 1 h. The copper surface area was measured by the method of N_2O dissociation of the catalyst samples [22]. A 150 mg catalyst sample was first reduced at 300 °C for 2 h, under a 10% H_2/He mixture flowing at 50 mL/min. The sample was cooled to 80 °C under a He flow, and a series of 100 μL of N_2O pulses were injected in a 10-min interval using He as a carrier gas (25 mL/min). The N_2 and N_2O in the effluent were separated in a Porapak N column (1.8 m, 1/8 inch) at room temperature and analyzed with a TCD detector.

RESULTS AND DISCUSSION

1. Catalyst Stability

The catalysts were subjected to three consecutive runs to test their stability. The CO conversion profiles of the CuO-ZnO catalyst on forward WGS and real WGS reactions are presented in Fig. 1. CuO-ZnO and CuO-Cr_2O_3 catalysts were stable with a 1% decrease in the conversion of the second run, whereas CuO-ZrO_2 showed a slightly greater decrease in the conversion of 3%, and CuO-CeO_2 catalyst showed a decrease of about 11% in the second run. However, the conversion of all catalysts was stabilized after the first run, as the conversion profiles of the second and third runs were almost identical.

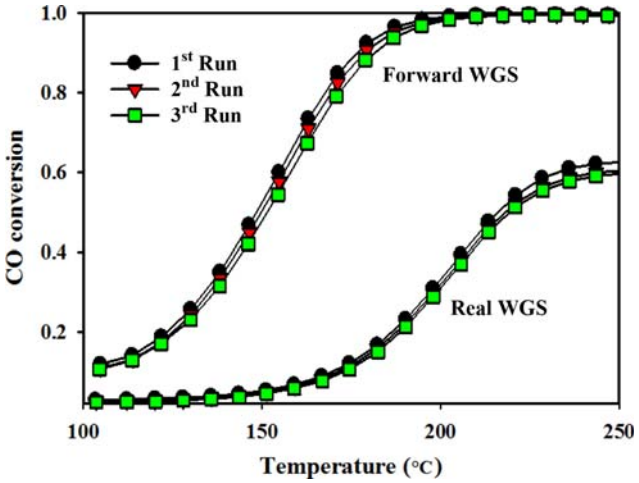

Fig. 1. CO conversion profiles of the CuO-ZnO catalyst in the three consecutive runs with the forward and real WGS feed.

2. Forward WGS

To eliminate the effect of product components (CO_2 and H_2) on WGS, the experiments were performed with the forward WGS feed (5% CO, 15% H_2O and balance He), and the results of which are shown in Fig. 2. CO conversion profiles for the prepared catalysts were compared with the profile of a commercial LTS catalyst (ICI 83-3). Among the catalysts, CuO-Cr_2O_3 exhibited the best performance with the forward WGS feed. Even at 100 °C, the CO conversion was 45% for CuO-Cr_2O_3, 26% for CuO-ZrO_2, 18% for CuO-CeO_2, 11% for CuO-ZnO and 5% for the commercial LTS catalyst (ICI 83-3). Up to 170 °C, all four catalysts showed higher CO conversion than ICI 83-3, while above 220 °C, all catalysts showed 100%

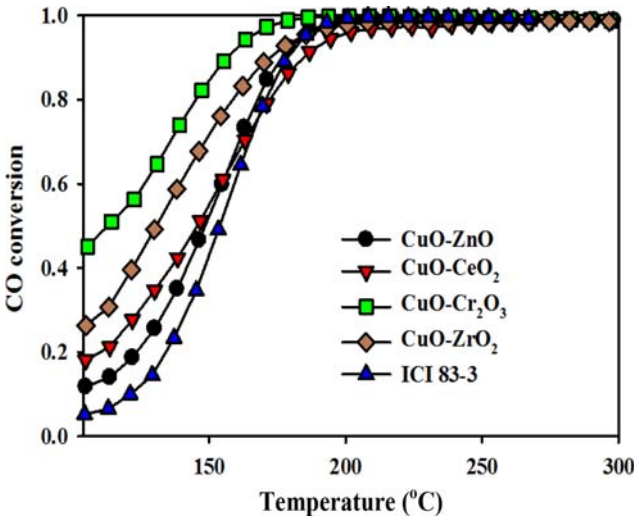

Fig. 2. CO conversion profiles of the catalysts with the forward WGS feed (5% CO, 15% H_2O and balance He; 50 ml/min).

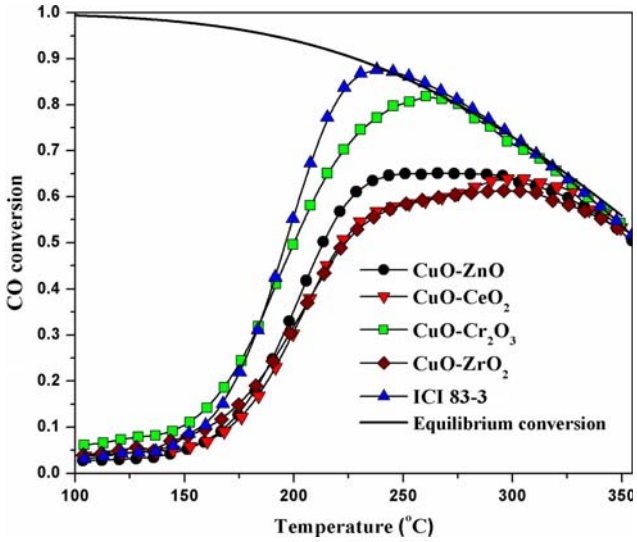

Fig. 3. CO conversion profiles of the catalysts with the real WGS feed (5% CO, 15% H_2O, 10% CO_2, 40% H_2 and balance He; 50 mL/min).

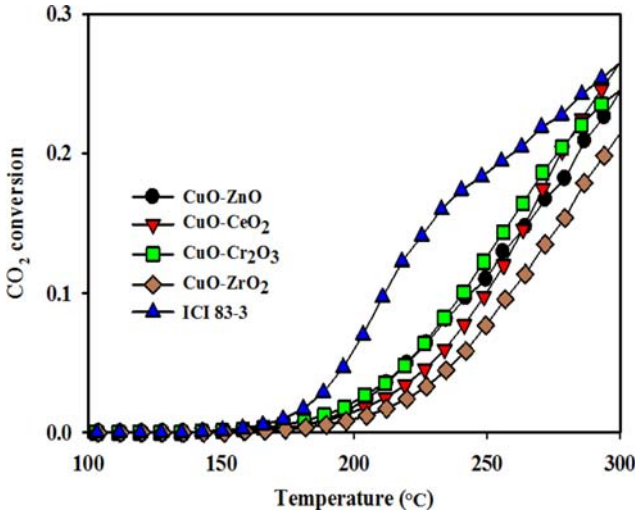

Fig. 4. CO_2 conversion profiles of the catalysts with the reverse WGS feed (40% H_2, 10% CO_2 and balance He; 50 ml/min).

CO conversion.

3. Real WGS

In addition to CO and H_2O, reformer effluents contain considerable amounts of CO_2 and H_2 (the product components of WGS). To examine the effect of these product components on WGS, the feed for the real WGS experiments was composed of 5% CO, 15% H_2O, 10% CO_2, 40% H_2 and balance He, with a total flow of 50 mL/min. The CO conversion profiles of the catalysts for real WGS reaction are shown in Fig. 3. The equilibrium CO conversion for the feed is also included in the figure. When compared to the case of the forward WGS (Fig. 2), the CO conversion decreased considerably in the presence of CO_2 and H_2. Above 200 °C, the commercial catalyst ICI 83-3 (having the composition: 51% CuO, 31% ZnO, 18% Al_2O_3) showed the best performance among the tested catalysts. Also, in this temperature range, the reverse WGS became increasingly significant with the reaction temperature, and hence, the measured CO conversion followed the equilibrium CO conversion above 225 °C and 250 °C for the commercial catalyst and CuO-Cr_2O_3, respectively.

There can be two possible causes for the considerable decrease in the CO conversion below 200 °C with the real WGS feed, as compared to the case with the forward WGS feed. As the WGS reaction is a reversible reaction, the product components in the real WGS feed can make the reverse WGS active, even below 200 °C, to form CO from CO_2 and H_2 in the feed, reducing the CO conversion of the WGS. The other possible cause for the decrease is an inhibition of the forward WGS by CO_2 and H_2, such as competitive adsorption of the product components on the active sites for the forward WGS. These two possibilities are experimentally examined in the next two sections.

4. Reverse WGS

To determine the effect of product components in the real WGS reaction, we studied the activity of catalysts for the reverse WGS reaction: $CO_2+H_2 \rightarrow CO+H_2O$. Fig. 4 shows the CO_2 conversion of the catalysts with the reverse WGS feed (40% H_2, 10% CO_2 and balance He). No appreciable CO_2 conversion was observed for any catalyst until 175 °C, showing that the reaction rate of the reverse WGS was negligibly slow. This clearly shows that the decrease in the CO conversion by switching the feed from the forward WGS to the real WGS was not caused by the reverse WGS.

Above 200 °C, the reverse WGS became more rapid with increasing temperature. The commercial catalyst (ICI 83-3) was the most active catalyst in the reverse WGS. The activity of CuO-Cr_2O_3, CuO-CeO_2 and CuO-ZnO was similar, and slightly better than that of CuO-ZrO_2 in the reverse WGS. In the case of CuO-Cr_2O_3 and ICI 83-3, the reverse WGS balanced the forward WGS reaction at high temperatures, as depicted in Fig. 3, so that once the conversion touched the equilibrium curve, it followed the equilibrium path.

5. Effect of CO_2 and H_2

To examine the individual effect of CO_2 and H_2 on WGS, either CO_2 or H_2 was added to the forward feed of 5% CO and 15% H_2O,

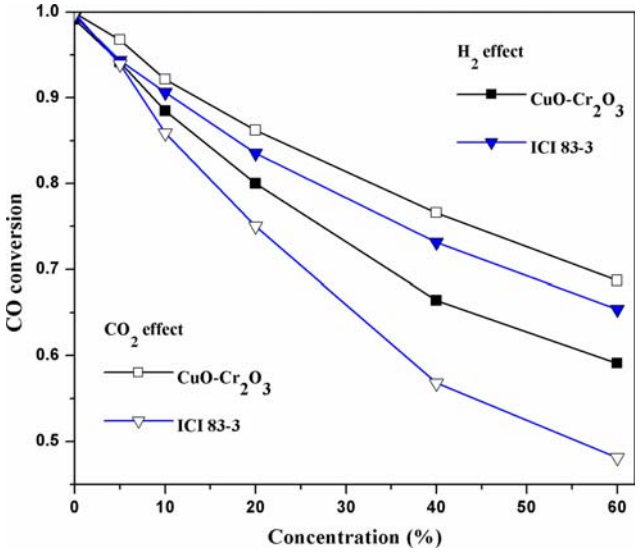

Fig. 5. Effect of CO_2 and H_2 on CO conversion at 180 °C with the forward WGS feed.

and its effect on the CO conversion was measured at 180 °C, where, in the absence of the product components, the CO conversion by the forward WGS was close to 1 (Fig. 2) and, in the presence of only the product components, the reverse WGS was negligible (Fig. 4). The content of CO_2 or H_2 in the feed was increased from 0 to 60% by volume (Fig. 5). The CO conversion decreased with increasing CO_2 or H_2 concentration in the feed. The result clearly shows that CO_2 and H_2 inhibited the forward WGS, and this effect of inhibition caused a considerable decrease in the CO conversion when switching the feed from the forward WGS to the real WGS feed. The inhibition effect was reversible, as the CO conversion returned to the same level as that of forward WGS when CO_2 or H_2 in the feed was replaced by He. This may suggest that CO_2 and H_2 are also adsorbed on the active sites of the catalysts, competing with CO and H_2O, and thus, inhibiting the forward WGS.

The extent of decrease in the CO conversion, however, also depended on the catalyst and the product component in the feed. For CuO-Cr_2O_3 catalyst, the decrease in the CO conversion was more pronounced for the feed containing H_2 than for that containing CO_2. However, for the commercial catalyst, the decrease was more pronounced for the feed which contained CO_2 than for that which contained H_2. In the real WGS condition, the feed contained much more H_2 than CO_2. For such a feed, the catalyst less susceptible to H_2 inhibition would perform better, and thus, the commercial catalyst showed better activity than CuO-Cr_2O_3.

6. Effect of Cu Loading in CuO-Cr_2O_3

The composition of commercial catalyst (ICI 83-3) is 53 wt% CuO, 31 wt% ZnO and 16 wt% Al_2O_3, whereas all the prepared catalysts in this work consisted of 30 wt% CuO with the remainder composed of the partner metal oxide. For a comparison between catalysts of similar Cu content, a 50 wt% CuO-Cr_2O_3 catalyst was prepared and tested for the real WGS reaction. Fig. 6 shows the performance of ICI 83-3, 50 wt% CuO-Cr_2O_3 and 30 wt% CuO-Cr_2O_3. Below 300 °C, the 50 wt% CuO-Cr_2O_3 exhibited a better CO conversion than the 30 wt% CuO-Cr_2O_3. Below 210 °C, the 50 wt% CuO-Cr_2O_3 also showed better performance than that of ICI 83-3. For a similar Cu content of 50 wt%, the CuO-Cr_2O_3 may substitute the commercial catalyst, particularly below 210 °C.

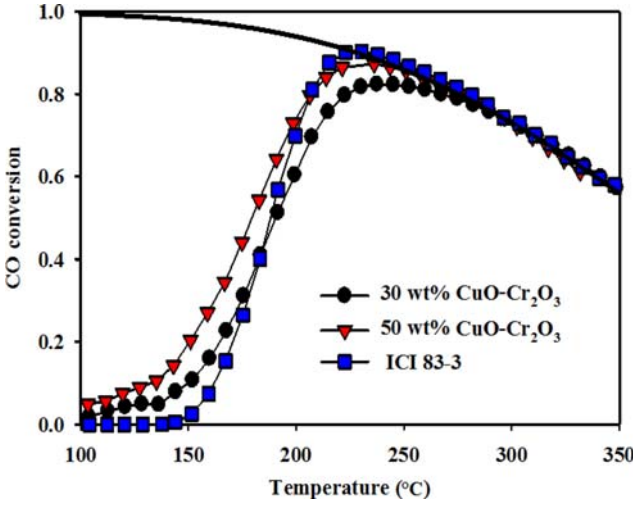

Fig. 6. CO conversion profiles of the catalysts (30 wt% CuO/Cr_2O_3, 50 wt% CuO/Cr_2O_3, ICI 83-3) with the real WGS feed.

Table 1. BET surface areas and copper metal surface areas of the catalysts

Catalyst	BET surface area (m^2/g)	copper metal surface area (m^2/g)
30 wt% CuO-ZnO	12	3.6
30 wt% CuO-CeO_2	69	-
30 wt% CuO-Cr_2O_3	17	4.6
30 wt% CuO-ZrO_2	96	2.7
ICI 83-3	74	5.8
50 wt% CuO-Cr_2O_3	15.5	6.1

7. Catalyst Characterization

7-1. BET Surface Area and Cu Metal Surface Area

The BET surface areas and the Cu metal surface areas were measured by the N_2O pulse dissociation method, and the results for each catalyst are listed in Table 1. Among the prepared catalysts, CuO-ZrO_2 catalyst has the largest surface area of 96 m^2/g and CuO-ZnO catalyst has the smallest area of 12 m^2/g. However, CuO-Cr_2O_3 (17 m^2/g) showed the best performance in the WGS reactions among all 30 wt% CuO catalysts, indicating that the BET area was not a key factor affecting the catalytic activity. The Cu metal areas of the catalysts in the table were also not correlated with the BET area. For the CuO-CeO_2 catalyst, it was not possible to measure the Cu metal area because the partner metal oxide CeO_2 repeatedly reduced the oxidized Cu species by the N_2O pulses, and hence the total amount of dissociated N_2O did not directly correspond to the total surface Cu metal [23].

Among the 30 wt% CuO catalysts, CuO-Cr_2O_3 was determined to have the largest Cu metal area of 4.6 m^2/g and was the most active catalyst in the forward WGS. Even in the forward WGS, the higher Cu metal area did not always result in a higher activity, since the commercial catalyst with the Cu metal area of 5.8 m^2/g was inferior to all the other catalysts below 170 °C (Fig. 2). For the real WGS condition (Fig. 3), however, the order in the Cu metal area of the catalysts was observed to be the same as the order in the catalytic performance above 200 °C, i.e., the commercial catalyst (5.8 m^2/g)> CuO-Cr_2O_3 (4.6 m^2/g)>CuO-ZnO (3.6 m^2/g)>CuO-ZrO_2 (2.7 m^2/g) CuO-CeO_2. This suggests that the Cu metal area of the catalyst significantly affects the catalytic activity, particularly under realistic WGS conditions.

7-2. XRD Analysis

Fig. 7(a)-(d) shows the XRD patterns of fresh and used catalysts after WGS reaction in both forward and real conditions. The crystal structure of copper in each catalyst has been marked in Fig. 7(a)-(d). All fresh catalysts showed a monoclinic CuO phase, except for CuO-Cr_2O_3, in which copper was observed as spinel copper chromate ($CuCr_2O_4$). After the reaction, copper chromate crystals were no longer present, being replaced by metallic copper and chromium oxide peaks. After the reaction, metallic Cu was observed in all catalysts and the corresponding peaks are indicated in Fig. 7. This is in agreement with previous studies [16,24,25] which have reported that metallic Cu is the active species in WGS.

7-3. H_2-TPR Studies

The reduction properties of the catalysts were measured by H_2-TPR experiments (Fig. 8). The peak temperature of the reduction

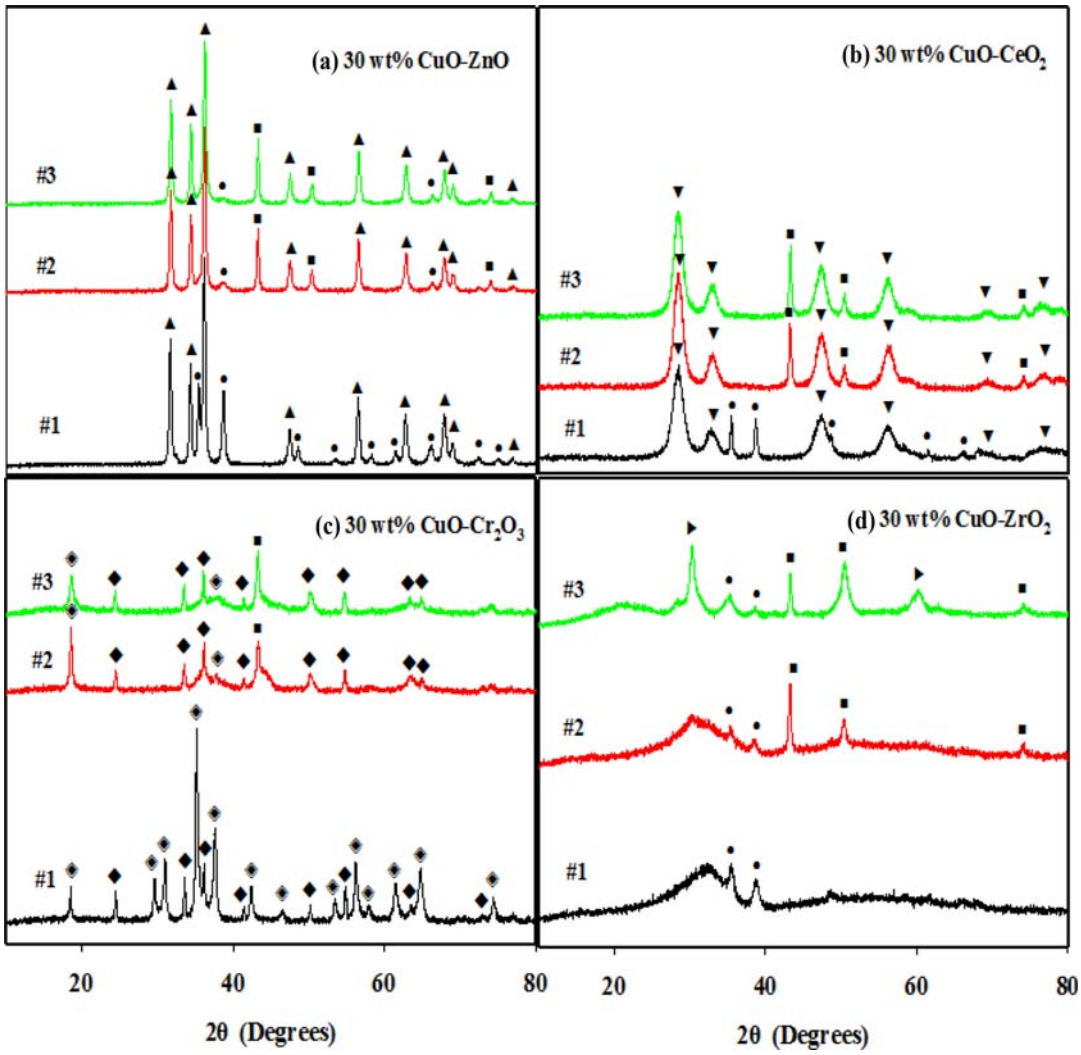

Fig. 7. XRD patterns of the prepared catalysts before and after reaction.
CuO - [●], ZnO - [▲], CeO_2 - [▼], Cr_2O_3 - [◆], $CuCr_2O_4$ - [◈], ZrO_2 - [▶], copper - [■]
#1 - fresh catalyst, #2 - after forward WGS reaction, #3 - after real WGS reaction

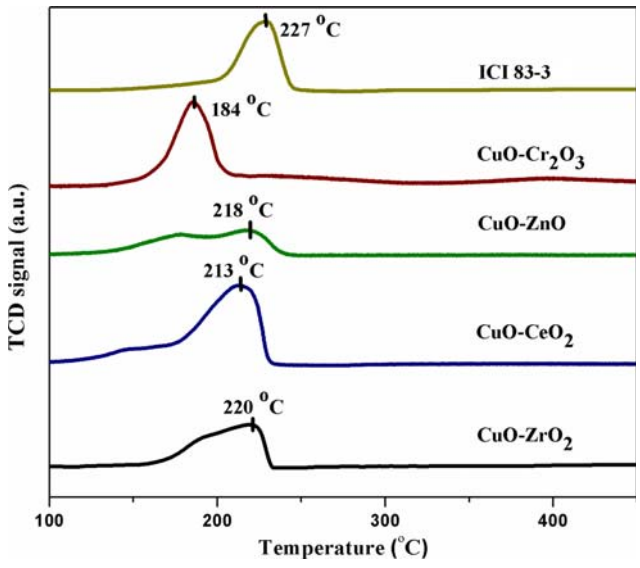

Fig. 8. H_2-TPR profiles of the catalysts.

profile of ICI 83-3 was 227 °C and was higher than those for the prepared 30 wt% CuO catalysts. The lowest peak temperature was observed for 30 wt% CuO-Cr_2O_3 at 184 °C, substantially lower than the peak temperatures of the other prepared catalysts. The low reduction temperature may indicate that the copper in CuO-Cr_2O_3 was highly dispersed, interacting strongly with the partner metal oxides to form $CuCr_2O_4$ spinel, as confirmed by XRD, and may have been responsible for high activity in the forward WGS.

CONCLUSIONS

30 wt% CuO-MO_x (M=Ce, Zn, Cr, or Zr) catalysts prepared by co-precipitation method as well as a commercial catalyst (ICI 83-3) were examined for their catalytic activity in the water gas shift (WGS) reaction under the forward (5% CO, 15% H_2O and balance He), reverse (40% H_2, 10% CO_2 and balance He), and real WGS feed (5% CO, 15% H_2O, 40% H_2, 10% CO_2 and balance He) conditions. For the forward feed, CuO-Cr_2O_3 showed the best performance among all catalysts, while ICI 83-3 was the most effective catalyst

for the real and reverse WGS feed.

When the feed was switched from the forward WGS feed to the real WGS feed containing the product components, CO_2 and H_2, the CO conversion was significantly suppressed in the temperature range of 100-350 °C. The suppression of the CO conversion could be attributed to the reverse WGS at temperatures well above 200 °C, but below 200 °C, where the reverse WGS was negligible, it was found to be caused by CO_2 and H_2 inhibition on the forward WGS reaction. The inhibition effect increased with increasing CO_2 or H_2 contents in the feed and also depended on the catalyst. As to the strength of the inhibition, it was found that ICI 83-3>CuO-Cr_2O_3 for CO_2 inhibition, and CuO-Cr_2O_3>ICI 83-3 for H_2 inhibition. For an H_2-rich feed such as the real WGS feed, it was desirable for a catalyst to be less inhibited by H_2 than by CO_2. In this regard, ICI 83-3 outperformed 30 wt% CuO-Cr_2O_3 in the case of the real WGS even though 30 wt% CuO-Cr_2O_3 was considerably more active than ICI 83-3 in the case of the forward WGS.

The Cu content of the catalyst was also an important factor affecting the catalyst activity. In the case of the real WGS, 50 wt% CuO-Cr_2O_3 was more active than 30 wt% CuO-Cr_2O_3 and was also more active than ICI 83-3 below 200 °C.

ACKNOWLEDGEMENT

This work was supported Kyungpook National University Research Fund.

REFERENCES

1. W. Vielstich, A. Lamm and H. A. Gasteiger, *Handbook of fuel cells: Fundamentals, technology, applications*, Wiley, Ltd., 3 (2003).
2. P. V. D. S. Gunawardana, H. C. Lee and D. H. Kim, *Int. J. Hydrog. Energy*, **34**, 1336 (2009).
3. M. Levent, *Int. J. Hydrog. Energy*, **26**, 551 (2001).
4. L. Li, Y. Zhan, Q. Zheng, Y. Zheng, C. Chen, Y. She, X. Lin and K. Wei, *Catal. Lett.*, **130**, 532 (2009).
5. N. E. Amadeo and M. A. Laborde, *Int. J. Hydrog. Energy*, **20**, 949 (1995).
6. N. Schumacher, A. Boisen, S. Dahl, A. A. Gokhale, S. Kandoi, L. C. Grabow, J. A. Dumesic, M. Mavrikakis and I. Chorkendorff, *J. Catal.*, **229**, 265 (2005).
7. M. V. Twigg and M. S. Spencer, *Appl. Catal. A: Gen.*, **212**, 161 (2001).
8. I. Atake, K. Nishida, D. Li, T. Shishido, Y. Oumi, T. Sano and K. Takehira, *J. Mol. Catal. A: Chem.*, **275**, 130 (2007).
9. C. Rhodes, G. J. Hutchings and A. M. Ward, *Catal. Today*, **23**, 43 (1995).
10. R. Kam, C. Selomulya, R. Amal and J. J. Scott, *J. Catal.*, **273**, 73 (2010).
11. Y. Li, Q. Fu and M. Flytzani-Stephanopoulos, *Appl. Catal. B: Environ.*, **27**, 179 (2000).
12. T. Tabakova, V. Idakiev, J. Papavasiliou, G. Avgouropoulos and T. Ioannides, *Catal. Commun.*, **8**, 101 (2007).
13. X. Qi and M. Flytzani-Stephanopoulos, *Ind. Eng. Chem. Res.*, **43**, 3055 (2004).
14. H. Yahiro, K. Murawaki, K. Saiki, T. Yamamoto and H. Yamaura, *Catal. Today*, **126**, 436 (2007).
15. X. Wang, J. A. Rodriguez, J. C. Hanson, D. Gamarra, A. Martinez-Arias and M. Fernandez-Garcia, *J. Phys. Chem. B*, **110**, 428 (2006).
16. H. Oguchi, H. Kanai, K. Utani, Y. Matsumura and S. Imamura, *Appl. Catal. A: Gen.*, **293**, 64 (2005).
17. J. B. Ko, C. M. Bae, Y. S. Jung and D. H. Kim, *Catal. Lett.*, **105**, 157 (2005).
18. T. Shishido, M. Yamamoto, D. Li, Y. Tian, H. Morioka, M. Honda, T. Sano and K. Takehira, *Appl. Catal. A: Gen.*, **303**, 62 (2006).
19. S. Boumaza, A. Auroux, S. Bennici, A. Boudjemaa, M. Trari, A. Bouguelia and R. Bouarab, *Reac. Kinet. Mech. Cat.*, **100**, 145 (2010).
20. X. Huang, L. Ma and M. S. Wainwright, *Appl. Catal. A: Gen.*, **257**, 235 (2004).
21. S. W. Park, O. S. Joo, K. D. Jung, H. Kim and S. H. Han, *Korean J. Chem. Eng.*, **17**, 719 (2000).
22. J. W. Evans, M. S. Wainwright, A. J. Bridgewater and D. J. Young, *Appl. Catal.*, **7**, 75 (1983).
23. P. Zimmer, A. Tschope and R. Birringer, *J. Catal.*, **205**, 339 (2002).
24. V. Ramaswamy, M. Bhagwat, D. Srinivas and A. V. Ramaswamy, *Catal. Today*, **97**, 63 (2004).
25. P. C. Yang, X. H. Cai, L. Y. Zhao, Y. C. Xie, Y. Xie, T. Hu and J. Zhang, *Surf. Interface Anal.*, **35**, 810 (2003).